

# A Mission-Centric Cyber-Resilience Benchmark for Silent-Watch Operation of Electrified Ground-Platform Power Architectures

Hongyu Wu and Raul Rodriguez  
 Department of Electrical and Computer Engineering  
 Kansas State University, Manhattan, KS, USA, 66506

**Abstract**—Silent-watch operation makes electrified ground platforms depend on supervisory energy management because mission loads must be sustained from stored energy while the engine is off. This paper develops a mission-centric cyber-resilience benchmark for this operating mode. The benchmark connects battery state-of-charge (SOC) spoofing to mission outcomes rather than evaluating the attack only through detector response or control error. It combines a reduced-order DC-bus model, residual-based detection, fallback shedding, and four mission-facing metrics for endurance, critical-load service, unsafe-voltage exposure, and detection delay. The study shows that SOC spoofing creates a structured stealth-versus-impact envelope. Small biases have limited mission effect, intermediate biases create an endurance deficit bounded by a closed-form expression in bias magnitude, shed power, and average battery draw, and large biases disable the SOC-driven guard. The results also show that defense value depends on fallback depth, not detection alone. An undersized fallback action can leave the Defended case worse than the undefended Attacked case. MATLAB-to-Simulink parity across five regression scenarios provides a software-verified basis for OPAL-RT/EXataCPS hardware-in-the-loop testing.

**Index Terms**—Silent watch, cyber-physical resilience, electrified ground platform, mission-centric evaluation, SOC spoofing, hardware-in-the-loop.

## I. INTRODUCTION

Electrification of military ground platforms changes the threat surface that mission planners must reason about. A platform that previously relied on mechanical drive and auxiliary generation may now depend on a battery, a DC bus, and a supervisory controller that arbitrates between mission-critical loads, sheddable loads, and protective actions. Silent watch is a combat-vehicle energy-management problem in which the platform must sustain mission loads from limited stored energy while the engine is off [1]. In that operating mode, the supervisor becomes a consequential decision-maker because it determines when to preserve energy, when to serve sheddable demand, and when to protect the platform. If an adversary compromises the supervisor’s perception of state, the platform can lose endurance and critical-load service even when the physical plant remains intact.

This paper combines mission-centric cyber resilience, vehicle energy-management security, and cyber-physical testbed development. Mission-impact methods argue that cyber effects should be evaluated by their consequences for mission objectives rather than by intrusion counts or packet-level indicators

alone [2], and mission-aware security work shows that asset criticality can depend on mission phase and time [3]. This framing is appropriate for silent-watch operation because the operational question is not only whether an intrusion is detected, but whether the platform can still complete its assigned task. The Army Modernization Strategy places ground combat vehicles within the Army’s modernization portfolio [4], while prior combat-vehicle work treats silent watch and energy management as operationally important functions [1]. What remains missing is a compact benchmark that lets mission planners and defense developers compare attacks and defenses on a common mission-facing basis.

Civilian vehicle and battery cybersecurity studies establish the technical plausibility of the threat considered here, but they do not provide the mission-mode benchmark needed for silent-watch analysis. Prior surveys identify attack surfaces across vehicular communication, sensing, charging, energy-management, and battery-control layers [5]–[8]. Sensor-side and in-vehicle-bus studies show that spoofed or injected measurements can affect vehicle cyber-physical behavior [9], [10], and connected or hybrid electric-vehicle studies show that adversarial inputs can steer supervisory energy-management and powertrain-control decisions [11], [12]. These studies motivate the attack model, but their center of mass is civilian vehicles, charging systems, grid coupling, and powertrain control rather than the engine-off supervisory loop of a tactical silent-watch platform.

Power-system cyber-physical security provides the closest technical foundation for the measurement-integrity aspect of the problem. False data injection formalizes how manipulated measurements can mislead state-aware monitoring and control systems [13]. Moving target defense studies show how changing system parameters or communication assumptions can reduce an attacker’s effectiveness against power-grid cyber-physical systems [14]–[16]. Learning-based detectors have been studied for false-data-injection detection and localization [17], [18], but our recent work shows that incomplete-network-information attacks can defeat machine-learning detectors [19]. This motivates the present benchmark’s use of a transparent residual detector in its first version. A broader review of smart-grid cyber-physical attack and defense appears in [20].

Real-time cyber-physical testbeds provide a path for trans-

lating the benchmark beyond offline simulation. EV charging studies establish grid-coupled vehicle cybersecurity as a relevant attack surface [21], [22]. OPAL-RT-class and hardware-in-the-loop (HIL) co-simulation platforms have been used for smart-grid performance and cyber-attack studies [23], [24], EXata-coupled real-time simulation has been used to examine cyber-attack impacts on microgrid controllers [25], and EV powertrain HIL has been developed for cyber-physical security studies [26]. Our prior Typhoon-HIL work further demonstrates real-time implementation of CNN-based false-data-injection detectors [27]. These studies show that real-time deployment is feasible, but they do not target the silent-watch supervisory loop or report cyber effects through mission-facing quantities such as endurance, critical-load service, unsafe-voltage exposure, and detection delay.

This paper addresses this gap by proposing a reduced-order, architecture-level benchmark for silent-watch operation. The contributions are as follows.

- 1) We formulate a mission-centric cyber-resilience benchmark with four mission-facing metrics across three reference cases (Nominal, Attacked, and Defended) and two attack-window variants.
- 2) We characterize a three-regime stealth-versus-impact envelope under SOC-bias sweeps and derive a closed-form endurance bound for the delay regime.
- 3) We identify a fallback-depth design constraint. In the reported configuration, undersized fallback shedding leaves the Defended case worse than the undefended Attacked case until the post-alarm shed fraction exceeds 0.4.

The remainder of the paper is organized as follows. Section II defines the system, threat, and defense models. Section III describes the benchmark methodology and mission metrics. Section IV presents the main results, and Section V provides discussion and conclusion.

## II. SYSTEM AND THREAT MODELS

### A. Platform abstraction

The platform is modeled as a DC-bus-centered source-storage-load-control system, shown in Fig. 1. The energy store is a battery characterized by a capacity  $E$  and an instantaneous state of charge  $s(t) \in [0, 1]$ . An optional auxiliary source surrogate  $p_s(t)$  represents an APU or generator contribution and is held at zero in the silent-watch case of record. The load is decomposed into a critical demand  $P_c(t)$  (sensors, communications, crew systems) and a sheddable demand  $P_h(t)$  (climate control, comfort loads). A supervisory controller selects a shed fraction  $u_{\text{shed}}(t) \in [0, 1]$  that determines what portion of  $P_h(t)$  is actually served. The battery balances any net demand left after the source contribution. Bus voltage  $v(t)$  is represented by a low-order surrogate

$$v_{\text{eq}} = V_{\text{nom}} - k_v \max(0, P_{\text{net}}) - k_s \max(0, 1 - s/s_{\text{ref}}), \quad (1)$$

Bus voltage  $v(t)$  tracks this equilibrium through the first-order lag  $\tau_v \dot{v}(t) = v_{\text{eq}}(t) - v(t)$ . The unsafe-voltage band is defined

TABLE I  
BENCHMARK PARAMETERS USED IN ALL REPORTED RUNS. IDENTIFIERS MATCH THE SYMBOLS USED IN THE TEXT.

Symbol	Value	Description
$E$	24 kWh	nominal usable battery energy
$s_0$	0.80	initial SOC
$s_{\text{warn}}$	0.65	supervisor SOC warning
$s_{\text{crit}}$	0.20	mission-fail SOC
$V_{\text{nom}}$	650 V	nominal bus voltage
$V_{\text{warn}}$	590 V	soft-shed bus threshold
$V_{\text{min}}$	585 V	unsafe-band entry
$V_{\text{fail}}$	570 V	mission-fail voltage
$\tau_v$	0.20 s	bus first-order time constant
$k_v$	2 V/kW	voltage droop slope
$k_s$	35 V	low-SOC droop weight
$s_{\text{ref}}$	1.0	SOC reference for droop activation
$P_c$ baseline / step	10 / +2 kW	critical demand profile
$P_h$ baseline / step	6 / +4 kW	sheddable demand profile
$\tau_d$	0.08	detector residual threshold
confirmation window	5 s	detector debounce time
$\sigma_{s_m}$	0.015	SOC sensor noise std. dev.
$\sigma_{p_{\text{bat}}} / P_{\text{bat}}$	0.02	current sensor noise (rel.)
Mission horizon $T$	3600 s	silent-watch evaluation window
Integrator step $\Delta t$	0.10 s	fixed-step explicit Euler

by  $V_{\text{min}}$ , while mission abort triggers if  $s(t) \leq s_{\text{crit}}$  or  $v(t) \leq V_{\text{fail}}$ , with  $V_{\text{fail}} < V_{\text{min}}$ . Unless otherwise stated, all reported cases use the fixed parameter set listed in Table I.

This abstraction is architecture-level. It is sufficient for comparative benchmarking and remains easy to translate into Simulink and HIL implementations without introducing modeling commitments that the present scope does not justify. The numerical parameters are illustrative and are not drawn from any specific platform's controller; they are sized to a representative crewed ground vehicle with a 24 kWh nominal usable battery and a 60-minute silent-watch horizon for the headline study.

### B. Supervisor

The supervisor implements two protective paths that act on different signals. The first is a soft-shed driven by the supervisor's view of state of charge,  $s_m(t)$ , which becomes more aggressive as  $s_m(t)$  approaches a warning threshold  $s_{\text{warn}}$  and a critical threshold  $s_{\text{crit}}$ . The second is a soft-shed driven by the measured bus voltage, which engages when  $v(t)$  falls toward its unsafe band. In nominal operation  $s_m(t) = s(t)$  and the two paths reinforce one another. The distinction matters under attack because the two paths have different exposure surfaces, as discussed below.

### C. Threat model

The primary threat is state-of-charge spoofing at the supervisory interface. The true SOC  $s(t)$  is unchanged physically, but the supervisor receives a biased measurement

$$s_m(t) = s(t) + b_a(t) \quad (2)$$

during a specified attack window. The structure mirrors classical false-data-injection against state estimation, in which physical quantities are unchanged while the controller-visible

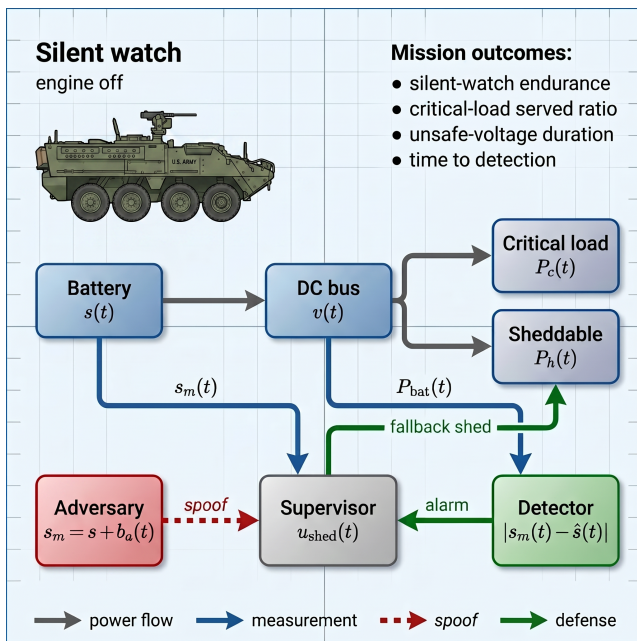


Fig. 1. Conceptual view of the silent-watch threat surface and the benchmark’s evaluation loop. A ground platform with the engine off sustains critical loads from stored energy alone (top). The supervisor arbitrates between critical and sheddable demand on the basis of the measured state of charge  $s_m(t)$ . A cyber adversary biases  $s_m$  during an attack window, which delays protective shedding and degrades mission endurance. A residual detector compares  $s_m$  against an independently propagated estimate  $\hat{s}(t)$  and triggers fallback shedding when the mismatch persists. The benchmark records four mission outcomes for every case: silent-watch endurance, critical-load served ratio, unsafe-voltage duration, and time to detection.

measurement is manipulated [13]. Battery-management threat surveys have explicitly identified state-of-charge as a high-value manipulation target because supervisory decisions depend on it directly [7]. Throughout this paper the bias is positive, so the supervisor overestimates available energy, delays protective action, and continues to support the sheddable load longer than is appropriate for the actual reserve. We consider two attack-window variants. The single-window variant applies the bias over [600, 2400] s. The multi-window variant applies the same bias across two disjoint intervals, [600, 1500] s and [2100, 2700] s (total 1500 s, versus 1800 s for the single-window case). This variant tests whether the benchmark response changes when spoofing is interrupted rather than continuous. Both variants share the headline bias of  $b_a = 0.50$  unless otherwise stated.

The headline configuration assumes a single concrete delivery channel: tampering of the supervisory state-of-charge message on the in-vehicle CAN bus, which is the channel for which sensor-bus injection has been studied most extensively in the connected-vehicle literature [9], [10]. The BMS threat literature also enumerates firmware compromise of the cell-monitoring stack and replay attacks on the energy-management bus [7], [8]. Each of those channels would inject the same biased  $s_m$  into the supervisor and is therefore covered by the same mission-level signature. The benchmark quantifies only

the platform-level consequence and does not attempt to attribute observed degradation to a specific delivery mechanism.

The threat is bounded to the SOC measurement channel. Coordinated multi-channel spoofing that simultaneously biases both the supervisor’s SOC reading and the predictor’s battery-current measurement would shrink the residual that the defense relies on; that case is excluded from the present scope and is identified in Section V as future work.

#### D. Defense

The defense layer combines a residual detector with a conservative fallback policy. A detector-side SOC predictor  $\hat{s}(t)$  is propagated from the measured battery-power balance and compared with  $s_m(t)$ . When  $|s_m(t) - \hat{s}(t)|$  exceeds a threshold  $\tau_d$  for the confirmation interval, an alarm is raised and the fallback controller reduces sheddable demand for the remainder of the mission. We use a residual detector because it makes the benchmark interpretable and separates mission impact from detector-family choice. To avoid a noise-free detector setting, the predictor uses noisy battery-current measurements (2% relative Gaussian noise) and  $s_m(t)$  includes additive SOC sensor noise ( $\sigma = 0.015$ ).

### III. BENCHMARK METHODOLOGY

#### A. Reference cases

Each scenario is exercised through three reference cases and two attack-window variants:

- **Nominal:** no attack, no defense. Establishes the energy-only mission envelope.
- **Attacked:** attack active, no defense. Establishes the unmitigated mission deficit.
- **Defended:** attack active, residual detector and fallback shed active. Establishes the mitigated mission envelope.

Note that, for sensitivity studies, the bias  $b_a$  and the fallback shed fraction are swept independently while all other parameters are held fixed.

#### B. Mission metrics

Four mission-facing metrics are proposed and recorded for every case:

- **Silent-watch endurance** (minutes): the time to mission abort, defined as  $s(t) \leq s_{\text{crit}}$  or  $v(t) \leq V_{\text{fail}}$ .
- **Critical-load served ratio:** the fraction of integrated critical demand actually delivered over the mission horizon.
- **Unsafe-voltage duration** (seconds): the time  $v(t)$  spends below its safe band.
- **Time to detection** (seconds): the elapsed time from attack onset to confirmed alarm. Reported as  $\infty$  when no alarm is raised.

These four metrics are deliberately mission-facing rather than control-theoretic. They allow platform stakeholders and control engineers to compare cases on a common footing. The benchmark prioritizes critical-load continuity; sheddable-load service is treated as the resource sacrificed by fallback control.

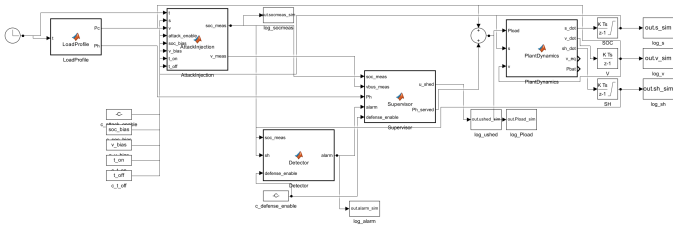


Fig. 2. Simulink implementation of the benchmark. Plant, supervisor, attack, and detector-plus-fallback are separate subsystems that mirror the conceptual architecture of Fig. 1.

TABLE II  
HEADLINE THREE-CASE COMPARISON,  $b_a = 0.50$ , SINGLE-WINDOW  
ATTACK ON  $[600, 2400]$  s.

Case	End. (min)	Crit. ratio	Unsafe (s)	Det. (s)
Nominal	47.92	0.996	215.15	$\infty$
Attacked	42.90	0.985	516.25	$\infty$
<b>Defended</b>	<b>58.40</b>	<b>1.000</b>	<b>0</b>	<b>5</b>

### C. Implementation and reproducibility

The implementation is organized around traceable benchmark cases rather than informal simulation runs. A MATLAB reference model defines the offline benchmark, and a Simulink model preserves the same state-update logic for later HIL execution. A regression harness runs both implementations on five regression scenarios and compares the mission-level outputs. This verifies the software translation before OPAL-RT/EXataCPS deployment, so later discrepancies can be attributed to HIL effects such as communication timing, I/O latency, or converter dynamics.

## IV. RESULTS

### A. Headline three-case comparison

Table II reports the four mission metrics for the three reference cases under the headline parameter set ( $b_a = 0.50$ , single-window attack on  $[600, 2400]$  s, 60-minute silent-watch horizon). Numbers are taken from the regression run that exercises both the MATLAB reference and the Simulink implementation.

The Nominal case carries 215 s of unsafe-voltage exposure because critical loads continue drawing near end of mission and the bus sags below  $V_{\min}$  as SOC approaches  $s_{\text{crit}}$ ; this is an inherent property of the rule-based supervisor, not a modeling artifact. Unsafe-voltage duration is therefore a stress-exposure metric; mission abort is governed by the SOC critical threshold  $s_{\text{crit}}$  or the lower voltage-failure threshold  $V_{\text{fail}}$ . The Attacked case more than doubles this exposure to 516 s by delaying protective shedding. The Defended case eliminates unsafe exposure entirely through the early fallback shed, restores critical service to unity, and extends endurance past Nominal at a 5 s detection latency. The multi-window variant reaches 41.74 min Attacked endurance and 708.85 s unsafe exposure under identical defense parameters; the Defended response is unchanged. The larger unsafe exposure reflects attack timing

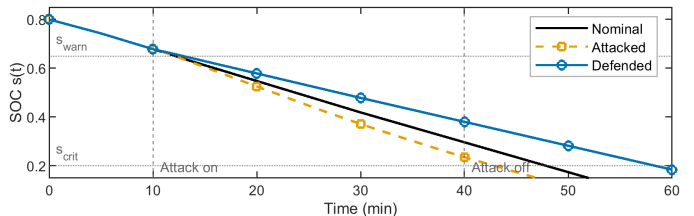


Fig. 3. Battery state of charge  $s(t)$  for the three reference cases. The Attacked case continues drawing on the sheddable load past the SOC warning threshold because the supervisor sees an inflated measurement.

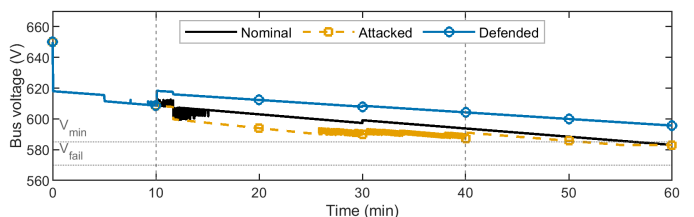


Fig. 4. Bus voltage  $v(t)$  for the three reference cases. The Attacked case spends more than twice as long below the safe band; the Defended case avoids the band entirely.

rather than total spoofing duration, because the later spoofing window acts when the battery and voltage margins are already smaller. Figs. 3 and 4 show the underlying SOC and bus voltage trajectories.

### B. Stealth-versus-impact regime structure

Fig. 5 reports the result of sweeping the bias  $b_a$  across  $[0, 0.6]$  while holding all other parameters fixed, with the three reference cases evaluated at each point. Three regimes are visible. Below approximately  $b_a = 0.04$  the residual remains under the detector's noise floor, the alarm does not fire, and the induced endurance loss in the Attacked case stays under 2% of the Nominal envelope. Between approximately  $b_a = 0.04$  and  $b_a = 0.45$  the detector fires within tens of seconds of attack onset, and the Defended case recovers to near-Nominal or higher endurance through fallback shedding. Above  $b_a \approx s_{\text{warn}} - s_{\text{crit}} = 0.45$  the SOC-measurement guard is fully blinded; the undefended Attacked case loses approximately 10% of endurance and spends roughly  $2.4\times$  as long in the unsafe band; the Defended case avoids both consequences through early fallback shedding.

The regime boundaries follow from the SOC threshold structure. In the delay regime, the biased SOC measurement postpones soft shedding until the true SOC has fallen approximately  $\Delta b = b_a - b_0$  below the nominal shed point, where  $b_0$  is the effective bias floor below which the mission effect is negligible. Let  $\bar{P}_{\text{bat}}$  denote the average net battery draw and  $P_{\text{shed}}$  denote the sheddable power  $P_h$  that would have been reduced at the soft-shed point under nominal operation. The shedding delay is then  $\Delta t_{\text{delay}} \approx \Delta b E / \bar{P}_{\text{bat}}$ . During this delay, the battery continues to serve  $P_{\text{shed}}$  beyond the post-shed load; the associated extra energy  $P_{\text{shed}} \Delta t_{\text{delay}}$  shortens the remaining

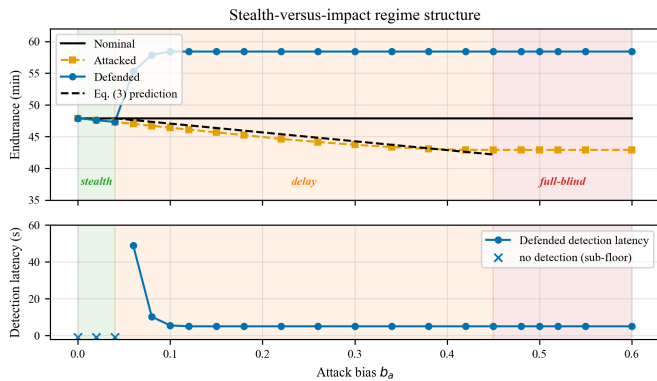


Fig. 5. Stealth-versus-impact regime structure obtained by sweeping the SOC-spoofing bias  $b_a$ . Top panel: silent-watch endurance for the three reference cases. Bottom panel: detection latency for the Defended case. Background bands mark the stealth (left), delay (center), and full-blind (right) regimes.

mission by approximately this extra energy divided by  $\bar{P}_{\text{bat}}$ . The endurance deficit therefore satisfies

$$\Delta \text{Endurance} \approx \frac{(b_a - b_0) P_{\text{shed}} E}{\bar{P}_{\text{bat}}^2}, \quad (3)$$

where  $b_0 \approx 0.04$  is the effective bias floor and  $E$  the nominal usable battery capacity. When  $E$  is in kWh and  $\bar{P}_{\text{bat}}$ ,  $P_{\text{shed}}$  are in kW, the bound carries units of hours. The predicted curve matches the observed delay-regime deficit in Fig. 5 with deviation below one minute. Under this threshold logic, the full-blind regime begins when the bias exceeds  $s_{\text{wam}} - s_{\text{crit}}$  (0.45 here). The benchmark therefore gives a compact analytical approximation of the attack envelope rather than only pointwise simulation comparisons.

### C. Cyber-physical defense-in-depth

The two protective paths in Section II have different exposure surfaces. The SOC-measurement-driven soft-shed is attackable through the measurement channel and is disabled under the full-blind attack. The voltage-driven soft-shed acts on plant state and is robust to measurement spoofing, but it engages only intermittently near the warning threshold. The residual-based defense bypasses both layers by acting on the prediction mismatch before the bus reaches its voltage guard. Any single protective path is insufficient; the combination of plant-driven and prediction-driven guards is what closes the gap.

### D. Fallback-depth sensitivity

A sweep of the fallback shed fraction from 0.2 to 1.0 under the large-bias attack reveals that the defense is not uniformly beneficial. Table III reports unsafe-voltage exposure and endurance for the Defended case across the swept depth.

At insufficient depth (0.2), the fallback action cannot lift the bus above its unsafe band. The Defended case then accumulates more unsafe-voltage exposure than the undefended Attacked case (810 s versus 516 s). Above a shed fraction of approximately 0.4, the defense becomes better than the undefended case; above 0.6, unsafe-voltage exposure is eliminated

TABLE III  
FALLBACK-DEPTH SENSITIVITY UNDER THE LARGE-BIAS ATTACK. DEFENDED-CASE ENDURANCE AND UNSAFE-VOLTAGE DURATION AS FUNCTIONS OF THE POST-ALARM SHED FRACTION.

Shed fraction	Defended endurance (min)	Defended unsafe (s)
0.2	44.54	810.25
0.4	48.24	195.65
0.6	52.76	0
0.8	58.40	0
1.0	60.00	0

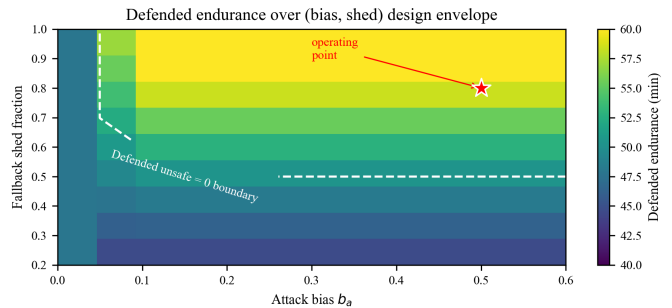


Fig. 6. Defended endurance over the joint (bias, fallback-shed-fraction) design envelope. The dashed contour marks the boundary of the unsafe-voltage-equals-zero region. The chosen operating point sits well inside the safe interior.

for this attack magnitude. The result establishes a minimum-viable-depth requirement as a transferable architectural constraint rather than a point-tuned setting.

The depth requirement generalizes naturally to the joint  $(b_a, u_{\text{shed}}^{\text{fb}})$  design space. Fig. 6 reports Defended-endurance over the (bias, shed-fraction) grid, with the Defended-unsafe-equals-zero boundary overlaid as a dashed contour. The chosen operating point  $(b_a, u_{\text{shed}}^{\text{fb}}) = (0.50, 0.80)$  sits well inside the unsafe-zero interior, which gives the defense margin against either an underestimated attack magnitude or a partially-failed shed actuator. The boundary itself slopes such that deeper shedding is required as bias grows, which is the expected direction.

### E. Preparation for HIL validation

The MATLAB reference and Simulink implementation were exercised on five regression scenarios, namely Nominal, Attacked, Defended, Attacked-multi, and Defended-multi. The two implementations use the same fixed step and state-update order. Across these scenarios, the mission metrics match exactly and the SOC and bus-voltage trajectory differences are zero to reported precision. This verifies the software translation before later OPAL-RT/EXataCPS experiments introduce communication timing, I/O latency, and converter dynamics.

## V. DISCUSSION AND CONCLUSION

The benchmark is intended for comparative mission evaluation rather than platform-specific endurance prediction. Because the reduced-order DC-bus model is used under a fixed

attack-defense setup, the reported quantities should be interpreted as changes in endurance, critical-load service, unsafe-voltage exposure, and detection delay, rather than as absolute claims about a particular vehicle. Within that scope, the results show that SOC spoofing can be mapped to mission-facing effects and that fallback depth is an architectural design variable rather than a post-alarm implementation detail.

The main findings are the structured attack envelope and the fallback-depth requirement. The bias sweep separates stealth, delay, and full-blind regimes. Small biases have limited mission effect, intermediate biases follow a closed-form endurance bound, and large biases disable the SOC-driven guard. The fallback-depth sweep shows that detection alone is insufficient. When fallback shedding is undersized, the Defended case can be worse than the Attacked case.

The MATLAB-to-Simulink parity result provides the software-verified basis for OPAL-RT/EXataCPS HIL evaluation. Future work will use this benchmark as a fixed baseline to test whether the attack-regime structure and fallback-depth requirement persist under higher-fidelity dynamics, communication timing effects, learning-based detection, and coordinated multi-channel adversaries.

## REFERENCES

- [1] M. S. Dattathreya and H. Singh, "Silent-watch and energy management strategy in combat vehicles," *IEEE Transactions on Aerospace and Electronic Systems*, vol. 50, no. 1, pp. 418–428, 2014.
- [2] S. Musman, A. Temin, M. Tanner, D. Fox, and B. Pridemore, "Evaluating the impact of cyber attacks on missions," The MITRE Corporation, Tech. Rep. Approved for Public Release Case 09-4577, 2010. [Online]. Available: <https://www.mitre.org/news-insights/publication/evaluating-impact-cyber-attacks-missions-0>
- [3] H. Cam and P. Mouallem, "Mission-aware time-dependent cyber asset criticality and resilience," in *Proceedings of the Eighth Annual Cyber Security and Information Intelligence Research Workshop (CSIIRW)*. ACM, 2013.
- [4] United States Army, "Army modernization strategy: Investing in the future," Department of the Army, Office of the Chief of Staff, 2019, public release; available at [army.mil](http://army.mil).
- [5] Z. El-Rewini, K. Sadatsharan, D. F. Selvaraj, S. J. Plathottam, and P. Ranganathan, "Cybersecurity challenges in vehicular communications," *Vehicular Communications*, vol. 23, p. 100214, 2020.
- [6] T. Aljohani and A. Almutairi, "A comprehensive survey of cyberattacks on EVs: Research domains, attacks, defensive mechanisms, and verification methods," *Defence Technology*, vol. 42, pp. 31–58, 2024.
- [7] S. Murlidharan, V. Ravulakole, J. Karnati, and H. Malik, "Battery management system: Threat modeling, vulnerability analysis, and cybersecurity strategy," *IEEE Access*, vol. 13, pp. 37 198–37 220, 2025.
- [8] F. Naseri, Z. Kazemi, P. G. Larsen, M. M. Arefi, and E. Schaltz, "Cyber-physical cloud battery management systems: Review of security aspects," *Batteries*, vol. 9, no. 7, p. 382, 2023.
- [9] Z. El-Rewini, K. Sadatsharan, N. Sugunaraj, D. F. Selvaraj, S. J. Plathottam, and P. Ranganathan, "Cybersecurity attacks in vehicular sensors," *IEEE Sensors Journal*, vol. 20, no. 22, pp. 13 752–13 767, 2020.
- [10] D. Kosmanos, A. Pappas, L. Maglaras, S. Moschoyiannis, F. J. Aparicio-Navarro, A. Argyriou, and H. Janicke, "A novel intrusion detection system against spoofing attacks in connected electric vehicles," *Array*, vol. 5, p. 100013, 2020.
- [11] L. Guo, B. Yang, J. Ye, H. Chen, F. Li, W. Song, L. Du, and L. Guan, "Systematic assessment of cyber-physical security of energy management system for connected and automated electric vehicles," *IEEE Transactions on Industrial Informatics*, vol. 17, no. 5, pp. 3335–3347, 2021.
- [12] L. Guo, J. Ye, and L. Du, "Cyber-physical security of energy-efficient powertrain system in hybrid electric vehicles against sophisticated cyberattacks," *IEEE Transactions on Transportation Electrification*, vol. 7, no. 2, pp. 636–648, 2021.
- [13] Y. Liu, P. Ning, and M. K. Reiter, "False data injection attacks against state estimation in electric power grids," in *Proceedings of the 16th ACM Conference on Computer and Communications Security (CCS '09)*. ACM, 2009, pp. 21–32.
- [14] K. R. Davis, K. L. Morrow, R. Bobba, and E. Heine, "Power flow cyber attacks and perturbation-based defense," in *2012 IEEE Third International Conference on Smart Grid Communications (SmartGridComm)*, 2012.
- [15] A. C. Pappa, A. Ashok, and M. Govindarasu, "Moving target defense for securing smart grid communications: Architecture, implementation & evaluation," in *2017 IEEE Power & Energy Society Innovative Smart Grid Technologies Conference (ISGT)*, 2017, pp. 1–5.
- [16] B. Liu and H. Wu, "Optimal D-FACTS placement in moving target defense against false data injection attacks," *IEEE Transactions on Smart Grid*, vol. 11, no. 5, pp. 4345–4357, 2020.
- [17] Y. He, G. J. Mendis, and J. Wei, "Real-time detection of false data injection attacks in smart grid: A deep learning-based intelligent mechanism," *IEEE Transactions on Smart Grid*, vol. 8, no. 5, pp. 2505–2516, 2017.
- [18] S. Wang, S. Bi, and Y.-J. A. Zhang, "Locational detection of the false data injection attack in a smart grid: A multilabel classification approach," *IEEE Internet of Things Journal*, vol. 7, no. 9, pp. 8218–8227, 2020.
- [19] B. Liu and H. Wu, "Low-rank false data injection attacks with incomplete network information against machine-learning detectors," *IEEE Transactions on Industrial Informatics*, vol. 21, no. 4, pp. 2868–2877, 2025.
- [20] H. Zhang, B. Liu, and H. Wu, "Smart grid cyber-physical attack and defense: A review," *IEEE Access*, vol. 9, pp. 29 641–29 659, 2021.
- [21] S. Acharya, Y. Dvorkin, and R. Karri, "Public plug-in electric vehicles + grid data: Is a new cyberattack vector viable?" *IEEE Transactions on Smart Grid*, vol. 11, no. 6, pp. 5099–5113, 2020.
- [22] S. Acharya, Y. Dvorkin, H. Pandžić, and R. Karri, "Cybersecurity of smart electric vehicle charging: A power grid perspective," *IEEE Access*, vol. 8, pp. 214 434–214 453, 2020.
- [23] D. Bian, M. Kuzlu, M. Pipattanasomporn, S. Rahman, and Y. Wu, "Real-time co-simulation platform using OPAL-RT and OPNET for analyzing smart grid performance," in *2015 IEEE Power & Energy Society General Meeting*, 2015, pp. 1–5.
- [24] Z. Liu, Q. Wang, Y. Tang, and M. Ni, "The real-time co-simulation platform with hardware-in-loop for cyber-attack in smart grid," in *2018 IEEE Innovative Smart Grid Technologies - Asia (ISGT Asia)*, 2018, pp. 845–849.
- [25] D. Pal and S. Singh, "Cyber-physical power system implementation using HYPERSIM and EXata to examine the impact of cyber-attack on microgrid controller," in *2023 IEEE International Conference on Power Electronics, Smart Grid, and Renewable Energy (PESGRE)*, 2023, pp. 1–6.
- [26] B. Yang, L. Guo, and J. Ye, "Real-time simulation of electric vehicle powertrain: Hardware-in-the-loop (HIL) testbed for cyber-physical security," in *2020 IEEE Transportation Electrification Conference & Expo (ITEC)*, 2020, pp. 63–68.
- [27] T. Aminov, H. Wu, B. Liu, and H. Zhang, "Real-time simulation of convolutional neural network detectors for false data injection attacks using typhoon HIL," in *2024 IEEE Kansas Power and Energy Conference (KPEC)*, 2024, pp. 1–6.